

Supporting information

Highly Efficient Photochemical Vapor Generation of Tellurium: Effects from Antimony and Ferric Ion

Weiwen Huang,[†] Ying Yu,[†] Liang Dong,[†] Xiuqin Deng,[†] Xinyi Zhao,[†] Liwei Liu^{*,††} and Ying Gao ^{*,†}

[†] State Key Laboratory of Geohazard Prevention and Geoenvironment Protection, College of Earth Sciences, Chengdu University of Technology, Chengdu, Sichuan 610059, China

^{††} State Key Laboratory of Vanadium and Titanium Resources Comprehensive Utilization, Pangang Group Research Institute Co., Ltd., Sichuan 617000, China

*Corresponding author E-mail: Ying.gaoy@gmail.com; sprinterxyz@163.com

Table of Contents

Figure S1. Signal response of 1.0 $\mu\text{g L}^{-1}$ Te(IV) and Te(VI) recorded by ICP-MS --	S3
Figure S2. The effect of UV irradiation time on the signal responses of 1.0 $\mu\text{g L}^{-1}$ Te(IV) and Te(VI) using a germicidal UV lamp -----	S4
Figure S3. The effect of Ar carrier gas flow rate of 1.0 $\mu\text{g L}^{-1}$ Te(IV)/Te(VI) responses -----	S5
Figure S4. UV-vis absorbance of the PVG medium -----	S6
Figure S5. Mass spectra of volatile Sb species generated by photochemical reduction -	S7
Figure S6. TEM characterization of nanoparticles in the liquid phase (without Te) -	S8
Figure S7. XPS spectra of the liquid solution after UV irradiation -----	S9
Figure S8. Comparison of sensitivity of different PVG systems of Te -----	S10
Table S1. ICP-MS operating conditions-----	S11
Table S2. GC-MS parameters-----	S12
Table S3. Comparison of the LODs of Te obtained in this study and previous reports -	S13
Text S1. Sample preparation for XPS analysis-----	S14
Text S2. Sample preparation for TEM-EDS analysis-----	S15
References -----	S16

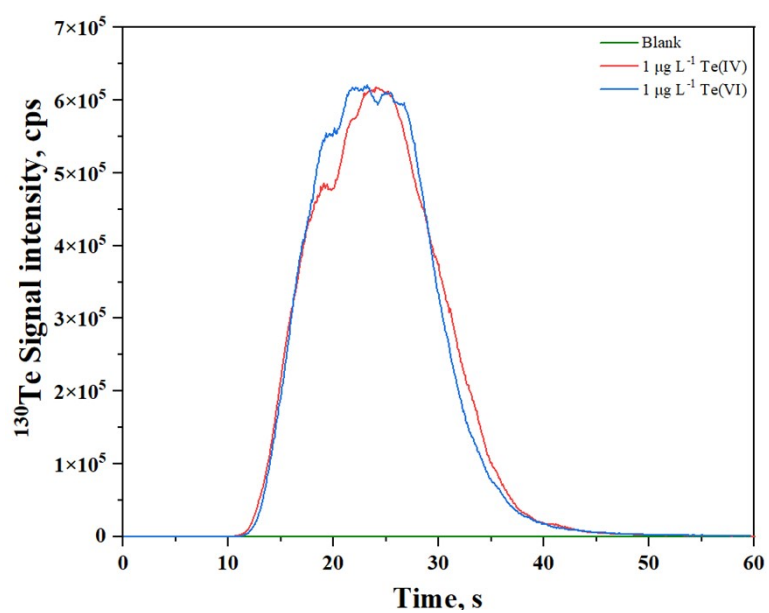


Figure S1. Signal response of $1.0 \mu\text{g L}^{-1}$ Te(IV) and Te(VI) recorded by ICP-MS (using collision mode with 2.4 mL min^{-1} He gas): 2% (v/v) AA, 5.0 mg L^{-1} Sb(III), 15.0 mg L^{-1} Fe(III), and 90 s irradiation time.

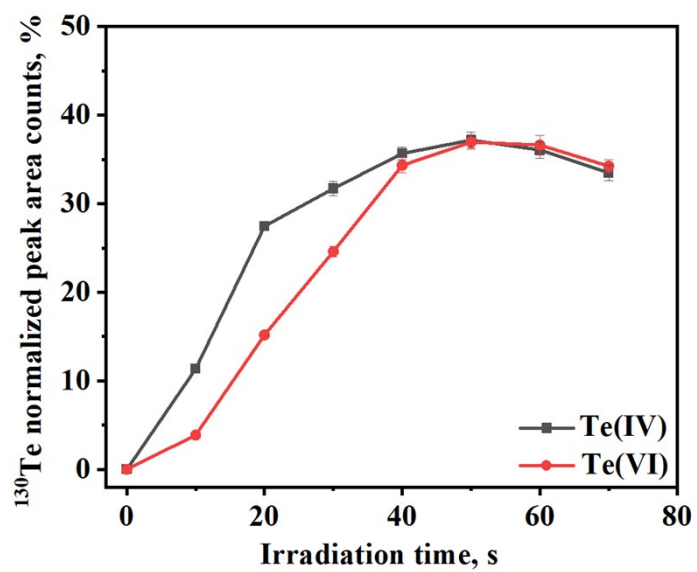


Figure S2. The effect of UV irradiation time on the signal responses of $1.0 \mu\text{g L}^{-1}$ Te(IV) and Te(VI) using a germicidal lamp: 5.0 mg L^{-1} Sb(III), 15.0 mg L^{-1} Fe(III), 2% (v/v) AA.

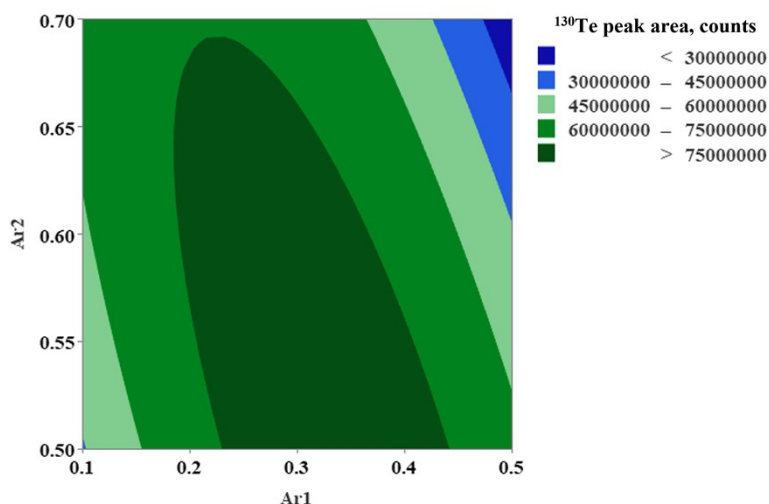


Figure S3. The effect of Ar carrier gas flow rate of $1.0 \mu\text{g L}^{-1}$ Te(IV)/Te(VI) responses: 5.0 mg L^{-1} Sb(III), 15.0 mg L^{-1} Fe(III), 2% (v/v) AA, 90 s irradiation time.

The flow rate of the carrier gas was found to significantly influence the separation efficiency of volatile species from the solution and the sampling depth of analytes in the plasma. In this study, a multivariate optimization technique was employed to investigate the effect of the argon carrier gas flow rate on the PVG reaction of $1.0 \mu\text{g L}^{-1}$ Te. Central composite design (CCD) was utilized to optimize the experimental procedure, construct the design matrix, and analyze the responses. A second-order polynomial quadratic model was established to analyze and interpret the relationship between the experimental results and the studied factors. Based on the calculation, the optimal reaction conditions were determined to be $\text{Ar}_1 = 0.3 \text{ L min}^{-1}$ and $\text{Ar}_2 = 0.6 \text{ L min}^{-1}$.

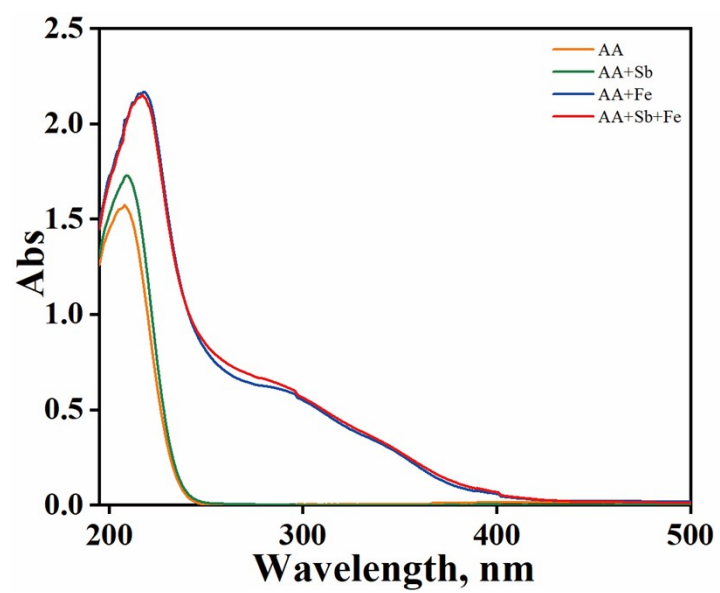


Figure S4. UV-vis absorbance of the PVG medium: 5.0 mg L⁻¹ Sb(III), 15.0 mg L⁻¹ Fe(III), 0.2% (v/v) AA.

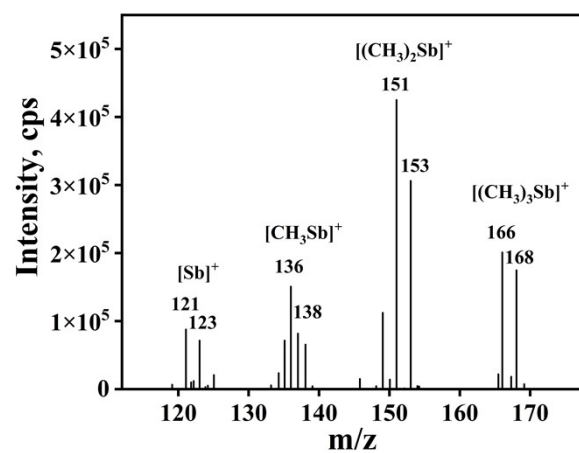


Figure S5. Mass spectra of volatile Sb species generated by photochemical reduction: 5.0 mg L^{-1} Te(IV), 5.0 mg L^{-1} Sb(III), 15.0 mg L^{-1} Fe(III), 2% (v/v) AA, and 90 s irradiation time.

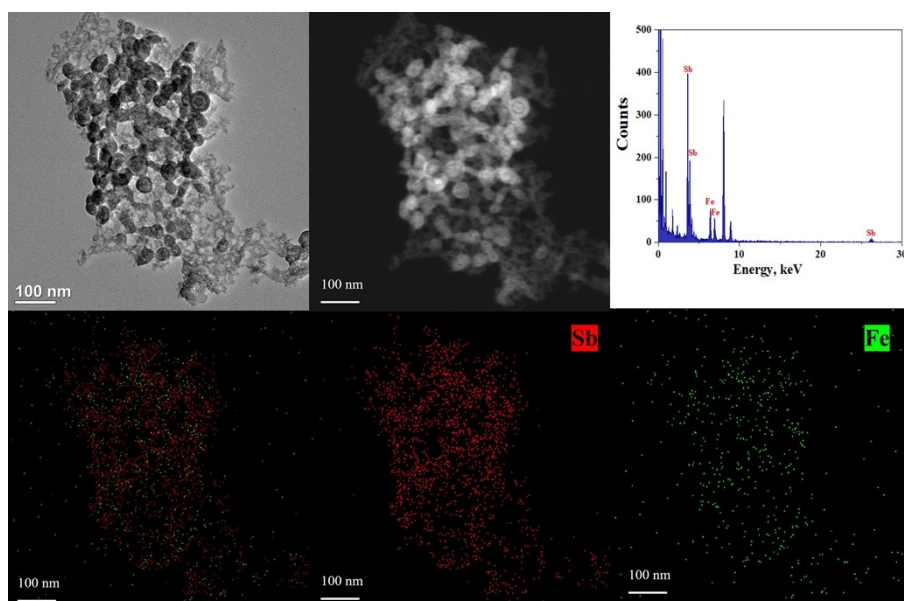


Figure S6. TEM characterization of nanoparticles in the liquid phase (without Te): 5.0 mg L⁻¹ Sb(III), 15.0 mg L⁻¹ Fe(III), 2 %(v/v) AA, 90 s irradiation.

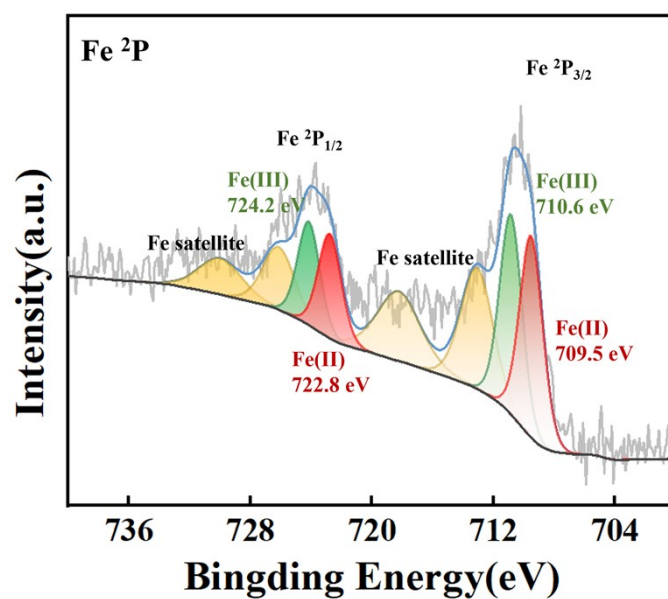


Figure S7. XPS spectra of the liquid phase products after UV irradiation: 10.0 mg L⁻¹ Te(IV), 15.0 mg L⁻¹ Sb(III), 40.0 mg L⁻¹ Fe(III), 10 %(v/v) AA, 90 s irradiation time.

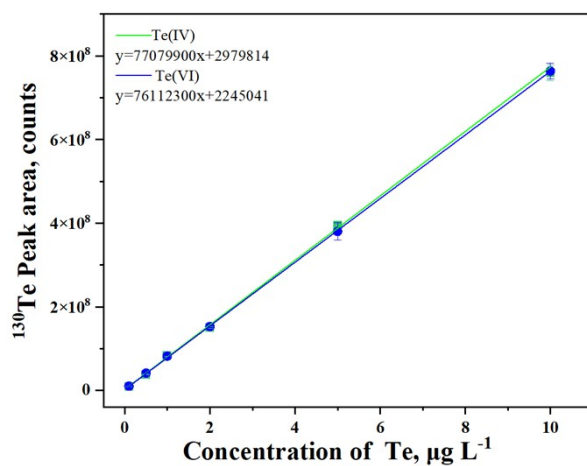


Figure S8. Calibration curves established by using the developed method with the ICP MS measurement (using collision mode with 2.4 mL min^{-1} He gas): 2% (v/v) AA, 5.0 mg L^{-1} Sb(III), 15.0 mg L^{-1} Fe(III), and 90 s irradiation time.

Table S1. ICP-MS operating conditions

Instrument settings	Value
RF generator power	1175 W
Ar carrier gas flow rate (PN)	1.10 L min ⁻¹
Ar carrier gas flow rate (PVG)	0.6 L min ⁻¹
Plasma flow rate	15 L min ⁻¹
He gas	2.4 mL min ⁻¹
Auxiliary gas flow rate	1.2 L min ⁻¹
Resolution	0.7 amu
Dead time	50 ns
Dwell time	30 ms
Scanning mode	Peak hopping
Sample flow rate	0.35 mL min ⁻¹
Isotope monitored	¹³⁰ Te

Table S2. GC-MS parameters

Instrument settings	Value
Capillary GC column	30 m×0.25 mm o.d.×0.25 µm i.d
Initial temperature	35 °C
Injector temperature	150 °C
Transfer line temperature	150 °C
He carrier gas flow rate	1.2 mL min ⁻¹
Furnace temperature program	Initial at 35°C, hold for 10 min, heated to 150 °C at 30 °C min ⁻¹
Split mode	10:1

Table S3. Comparison of the LODs of Te obtained in this study and previous reports

Method	Elemental valence	LOD/ ng L ⁻¹	Reference
PVG-AFS	Te(IV)	80	<i>Microchem J.</i> , 2010, 95 (1), 32-37. ¹
Fe/nano-TiO ₂ assisted PVG-ICP-MS	Te(IV)/Te(VI)	1.0	<i>Anal. Chem.</i> , 2018, 90 (9), 5737-5743. ²
Co ²⁺ assisted PVG-AFS	Te(IV)	60	<i>J. Anal. At. Spectrom.</i> , 2020, 35 (7), 1405-1411. ³
Fe ²⁺ /Mn ²⁺ assisted PVG-ICP-MS	Te(IV)	1.3	<i>Anal. Chim. Acta.</i> , 2022, 1201. ⁴
LS-AAS	Te(IV)	5.6 (µg L ⁻¹)	<i>Monatsh. Chem.</i> , 2022, 153 (9), 811-819. ⁵
HRCS-AAS	Te(IV)	0.85 (µg L ⁻¹)	
V(V) assisted PVG-ICP-MS	Te(IV)/Te(VI)	2.9	<i>Anal. Chem.</i> , 2022, 94 (11), 4770-4778. ⁶
PVG-ICP-MS	Te(IV)	0.7	<i>Talanta.</i> , 2018, 187, 370-378. ⁷
Co ²⁺ assisted PVG-ICP-MS	Te(IV)	0.6	<i>Geostand Geoanal Res.</i> , 2023, 48 (1), 133-143. ⁸
Sb/Fe assisted	Te(IV)/Te(VI)	0.4	This work

Text S1. Sample preparation for XPS analysis

A XPS was employed for the characterization of the products generated after the photochemical reaction. The relevant parameters were as follows: Monochromatic Al K α ($h\nu = 1486.6$ eV), power 150 W, beam spot size 650 μm , voltage 14.8 kV, current 1.6 A. Charge correction was performed using adventitious carbon C 1s = 284.8 eV for calibration. The whole process of sample collection was carried out in a glove box filled with argon gas. The sample solution was introduced into the photochemical reactor through continuous sampling. The flow rate of the sample was adjusted to ensure that the sample solutions in each system could receive 90 s duration of UV irradiation. An 8 cm-long polytetrafluoroethylene (PTFE) tube was connected to the outlet of the photochemical reactor. The nanoparticles formed in sample solution after UV irradiation would be adsorbed on the inner wall of the PTFE tube. Subsequently, the PTFE tube was cut into 1.0 cm \times 1.0 cm squares, exposing the adhered material on the inner tube walls. Finally, samples were placed in a chamber filled with Ar for XPS analysis. The composition of the sample solutions was as follows: 10.0 mg L $^{-1}$ Te(IV), 15.0 mg L $^{-1}$ Sb(III), 40.0 mg L $^{-1}$ Fe(III), and 10% (v/v) AA.

Text S2. Sample preparation for TEM-EDS analysis

The sample solution was introduced into the photochemical reactor through continuous sampling. The flow rate of the sample was adjusted to ensure that the sample solutions in each system could receive 90 s of UV irradiation. An 8 cm-long PTFE tube was connected to the outlet of the photochemical reactor. The nanoparticles formed in sample solution after UV irradiation would be adsorbed on the inner wall of the PTFE tube. Subsequently, the PTFE tube was cut and placed in 1.0 mL of ethanol solution and followed by ultrasonic dispersion treatment. A pipette was used to draw 5.0 μL of the solution and transfer it to the surface of a copper grid, followed by drying. This process was repeated 6 times. The composition of the sample solutions was as follows: 10.0 mg L^{-1} Te(IV), 5.0 mg L^{-1} Sb(III), 15.0 mg L^{-1} Fe(III), and 2% (v/v) AA.

References

1. C. Zheng, Q. Ma, L. Wu, X. Hou and R. E. Sturgeon, *Microchemical Journal*, 2010, **95**, 32-37.
2. H. He, X. Peng, Y. Yu, Z. Shi, M. Xu, S. Ni and Y. Gao, *Analytical chemistry*, 2018, **90**, 5737-5743.
3. W. Zeng, J. Hu, H. Chen, Z. Zou, X. Hou and X. Jiang, *Journal of Analytical Atomic Spectrometry*, 2020, **35**, 1405-1411.
4. E. Jeníková, E. Nováková, J. Hraníček and S. Musil, *Analytica Chimica Acta*, 2022, **1201**, 339634.
5. E. Jeníková, E. Nováková, H. Ruxová, S. Musil and J. Hraníček, *Monatshefte für Chemie-Chemical Monthly*, 2022, **153**, 811-819.
6. L. Dong, H. Chen, Y. Ning, Y. He, Y. Yu and Y. Gao, *Analytical chemistry*, 2022, **94**, 4770-4778.
7. K. A. Romanovskiy, M. A. Bolshov, A. V. Münz, Z. A. Temerdashev, M. Y. Burylin and K. A. Sirota, *Talanta*, 2018, **187**, 370-378.
8. Y. Yuan, Z. Han, F. Yang, H. Yu, Y. Zhang and M. Wen, *Geostandards and Geoanalytical Research*, 2024, **48**, 133-143.